

A Comparison of Residual Stress Development in Inertia Friction Welded Fine Grain and Coarse Grain Nickel-Base Superalloy

N. IQBAL, J. ROLPH, R. MOAT, D. HUGHES, M. HOFMANN, J. KELLEHER, G. BAXTER, P.J. WITHERS, and M. PREUSS

The effect of the base material microstructure on the development of residual stresses across the weld line in inertia friction welds (IFWs) of high-strength nickel-base superalloy RR1000 was studied using neutron diffraction. A comparison was carried out between tubular IFW specimens generated from RR1000 heat treated below (fine grain (FG) structure) and above (coarse grain (CG) structure) the γ' -solvus. Residual stresses were mapped in the as-welded (AW) condition and, after a postweld heat treatment (PWHT), optimized for maximum alloy strength. The highest tensile stresses were generally found in the hoop direction at the weld line near the inner diameter of the tubular-shaped specimens. A comparison between the residual stresses generated in FG and CG RR1000 suggests that the starting microstructure has little influence on the maximum residual stresses generated in the weld even though different levels of energy must be input to achieve a successful weld in each case. The residual stresses in the postweld heat treated samples were about 35 pct less than for the AW condition. Despite the fact that the high-temperature properties of the two parent microstructures are different, no significant differences in terms of stress relief were found between the FG and CG RR1000 IFWs. Since the actual weld microstructures of FG and CG RR1000 inertia welds are very similar, the results suggest that it is the weld microstructure and its associated high-temperature properties rather than the parent material that affects the overall weld stress distribution and its subsequent stress relief.

DOI: 10.1007/s11661-011-0802-0

© The Minerals, Metals & Materials Society and ASM International 2011

I. INTRODUCTION

NICKEL-base superalloys are used at high temperatures, in aggressive environments, and therefore are critical structural materials for aeroengine applications.^[1] Durability of these alloys is dependent on the retention of strengthening by γ' precipitates.^[2,3] RR1000 is a powder metallurgy nickel-base superalloy with a trimodal γ' size distribution when solution heat treated below the γ' -solvus, with γ' precipitation ranging from 30 nm to 1 μm , as shown in Figure 1. The alloy was developed specifically for use in aero engine applications with a maximum temperature capability of 725 °C (or 1000 K, hence RR1000).^[4] The nominal chemical

composition of RR1000 is given in Table I. This alloy resists cracking, corrosion, and oxidation when subjected to extreme heat, but is difficult to weld when using conventional joining methods. Therefore, inertia friction welding was developed successfully as a joining technique for this alloy.^[3,5-7] In essence,^[8] inertia friction welding is a joining process in which one of the work pieces is connected to a flywheel that provides the kinetic energy, while the other work piece is restrained from rotating. The flywheel is accelerated to a predetermined rotational speed and is then disengaged. At this point, the work pieces are forced together, resulting in generation of friction heat at the contact interface. In other words, the stored energy in the rotating flywheel is dissipated as heat through friction at the weld interface, resulting in a heat-affected zone (HAZ). At the same time, the axial welding pressure pushes out the soft material near the weld interface and a flash is formed. Ultimately, the rotation ceases and a solid-state bond is formed. Due to the high strain rates in the weld region, predicted to be in the range of 1 to 5 s⁻¹,^[9] dynamic recrystallization leading to grain refinement is usually observed in this region, as demonstrated in Reference 3. Since the volume of a work piece is typically large compared to the volume heated during the process, high cooling rates are obtained in the HAZ when the flywheel comes to a halt. This generates significant misfit strains between the weld regions and the parent material,

N. IQBAL and R. MOAT, Research Fellows, J. ROLPH, EngD Student, P.J. WITHERS, Professor of Materials Science, and M. PREUSS, Professor of Metallurgy, are with the School of Materials, University of Manchester, Manchester, M1 7HS, United Kingdom. Contact e-mail: michael.preuss@manchester.ac.uk D. HUGHES, formerly Beamline Scientist, with the Institute Laue Langevin, 38042 Grenoble Cedex 9, France, is now a Research Fellow, with the WMG, IARC, University of Warwick, Coventry, CV4 7AL, United Kingdom. M. HOFMANN, Beamline Scientist, is with Forschungsneutronenquelle Heinz-Maier Leibniz (FRM II), Technische Universität München, 85747 Garching, Germany. J. KELLEHER, Beamline Scientist, is with the ISIS, STFC, Rutherford Appleton Laboratory, Harwell Science and Innovation Campus, Didcot OX11 0QX, United Kingdom. G. BAXTER, Materials Specialist, is with Rolls-Royce plc., Derby DE24 8BJ, United Kingdom.

Manuscript submitted January 5, 2011.

Article published online September 13, 2011

leading to high residual stresses usually being observed in the HAZ.^[6,7,10] Cost-effective design and safety requirements for aeroengine turbine pose a fundamental challenge, demanding reasonably low levels of residual stress in the weld. Consequently, a postweld heat treatment (PWHT) is applied to reduce the residual stresses in the inertia friction weld (IFW) components to an acceptable level that, at the same time, does not deteriorate the mechanical properties of the specimen by significantly coarsening the γ' precipitates. It was demonstrated previously that the temperature capability of the nickel-base superalloy can have a significant effect on the residual stresses generated during inertia friction welding.^[10] This work showed that the maximum tensile stresses generated by IFW increased from those in INCONEL* 718 by

*INCONEL is a trademark of Special Metals Corporation, New Hartford, NY.

45 pct moving to alloy 720LI and by a further 50 pct moving to RR1000 (these alloys correspond to an increase in temperature capability of 323 K (50 °C) and 373 K (100 °C), respectively). In that case, the RR1000 material had a fine γ grain size ($\sim 5 \mu\text{m}$),^[3] since it had been solution heat treated below the γ' solvus. More recently, new processing routes for RR1000 were explored, resulting in an increased γ grain size in order to increase creep performance.^[11] This is achieved by solution heat treating the material above the γ' solvus: this translates into a further 303 K (30 °C) temperature capability increase compared to fine grain (FG) RR1000.^[4] Consequently, it is important to identify whether this increase of temperature capability results in a further increase of residual stresses when CG RR1000 is joined by inertia friction welding. In the present work, residual stresses in similar metal IFWs of RR1000 for

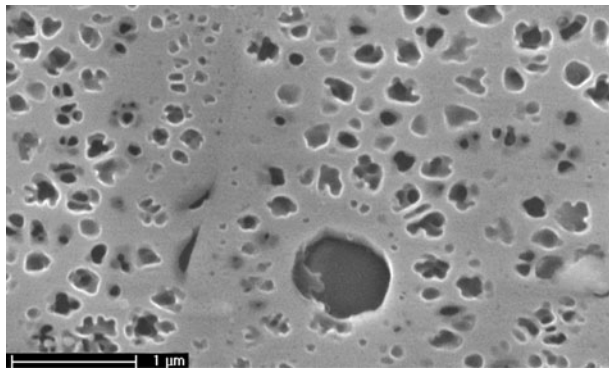


Fig. 1—SEM micrograph illustrates the size distribution of primary, secondary, and tertiary γ' precipitates in the nickel-base superalloy RR1000 when heat treated below the γ' solvus.

Table I. Chemical Composition (Weight Percent) of RR1000

Element	Ni	Cr	Co	Mo	Al	Ti	Ta	Hf	Zr	C	B
Wt pct	balance	18.5	18.5	5	3	3.6	2	0.5	0.06	0.027	0.015

coarse grain (CG) and FG material were investigated by neutron diffraction. In addition to the residual stress characterization of the as-welded (AW) conditions, the effect of the different parent material microstructures on stress mitigation during PWHT was investigated.

II. EXPERIMENTAL

Four inertia friction welded RR1000 tubes having an outer diameter (OD) of 143 mm and wall thickness of 8 mm after subsequent machining of the flash were provided by Rolls Royce plc (Derby, United Kingdom). The IFWs were produced on a development inertia friction welder at MTI (South Bend, IN). The microstructural condition of the base material and the heat treatment conditions for each specimen (S1-S4) are described in Table II. In all cases, the material was in a partially aged condition in order to provide a large enough process window for a subsequent PWHT. Weld parameters were chosen with the aim of obtaining similar upset for CG and FG IFWs. This was achieved by increasing the weld energy but keeping the weld pressure constant. Welds of the same parent microstructure were welded using the same welding parameters. The PWHT applied for this study was a development heat treatment aimed at minimizing any loss of mechanical strength to the alloy.

In order to determine the residual stress field near the weld boundary by neutron diffraction, it was necessary to measure the residual strain in the three perpendicular directions, namely, the hoop, axial, and radial directions (Figure 2). The alignment of the samples with respect to the incoming and diffracting beam is illustrated schematically in Figure 3. At research reactors, stress mapping is usually undertaken using a monochromated beam. Consequently, the residual stress is based on a single reflection and the choice of reflection is critical as a linear elastic strain response is only found for diffraction peaks that are least prone to intergranular strain development. By contrast, in the case of time-of-flight instruments at spallation sources, the measured diffraction spectrum, rather than a single reflection, is used to determine the lattice parameter, a , by applying a Rietveld refinement.^[12] Either way, strain is calculated

Table II. Summary of the IFW, Measured at SALSA (ILL), ENGIN-X (ISIS), and STRESS SPEC (FRM II)

Specimen	Microstructure	Condition
S1	CG	AW
S2	CG	PWHT
S3	FG	AW
S4	FG	PWHT

by using the standard engineering strain equation and requires a strain-free reference value. In most welded components, the value of the strain-free lattice spacing/parameter is by no means constant across the component. This is related to microstructural variations, which are associated with the chemical changes of the measured phase. Since even small chemical variations can result in significant shifts of the diffraction peak, an accurate strain analysis based on diffraction techniques requires a careful consideration of d_0/a_0 variations. More details about this issue can be found in Reference 13. In the case of the IFWs, it was shown previously^[7] that an axial stress balance model can be applied to take the d_0 variations into account across the weld line assuming microstructural variations occur predominantly with axial distance from the weld line rather than across the wall thickness. Detailed microstructure

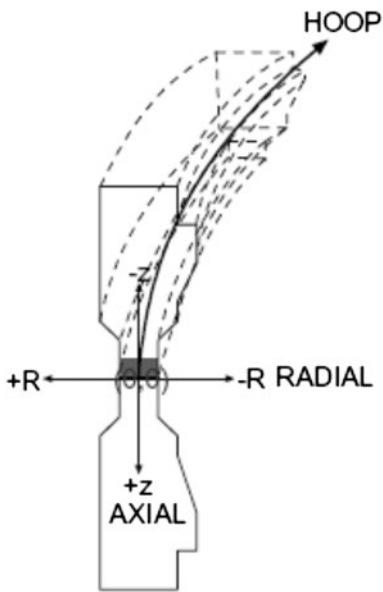


Fig. 2—Coordinate system, for the measured cross section, of IFW specimens. The shaded area illustrates the region where residual stress measurements were made.

studies and d_0 measurements showed that this is a valid assumption.^[3] Consequently, the strain for all neutron diffraction measurements was calculated using

$$\varepsilon = \frac{d - d_0(z)}{d_0(z)} = \frac{a - a_0(z)}{a_0(z)} \quad [1]$$

where ε is the measured strain and $d_0(z)$ and $a_0(z)$ are the axial position dependent strain free lattice spacing/parameter. Once the strain is known in the three perpendicular directions, the corresponding hoop, radial, and axial stresses are calculated using^[14,15]

$$\sigma_{\text{hoop}} = \frac{E}{(1 + \nu)(1 - 2\nu)} \times [(1 - \nu)\varepsilon_{\text{hoop}} + \nu(\varepsilon_{\text{radial}} + \varepsilon_{\text{axial}})], \text{ etc.} \quad [2]$$

where E is represented by the plane-specific diffraction elastic constant when using a single peak analysis and the bulk Young's modulus when using a Rietveld analysis. Similarly, either a diffraction plane specific value or the bulk value of Poisson's ratio, ν , was used. The elastic constants used in the present study for RR1000 are summarized in Table III.

The neutron diffraction measurements of postweld heat-treated samples (S2 and S4) were performed on the diffractometer SALSA^[16] at the Institute Laue Langevin (ILL, research reactor) in Grenoble, France. Sample S3 (FG-AW) was measured on the time-of-flight spectrometer ENGIN-X^[17] (ISIS), while sample S1 (CG-AW) was measured on the STRESS SPEC beam line^[18] at FRM II (research reactor) in Munich, Germany. It is

Table III. Elastic Constants of RR1000 Used to Convert Strain to Stress; the (311) Diffraction Elastic Constants are Based on Unpublished Results from *In-Situ* Loading Experiments Using Neutron Diffraction

Young's modulus	226 GPa
Poisson ratio	0.26
(311) diffraction elastic constant	200 GPa
(311) Poisson ratio	0.24

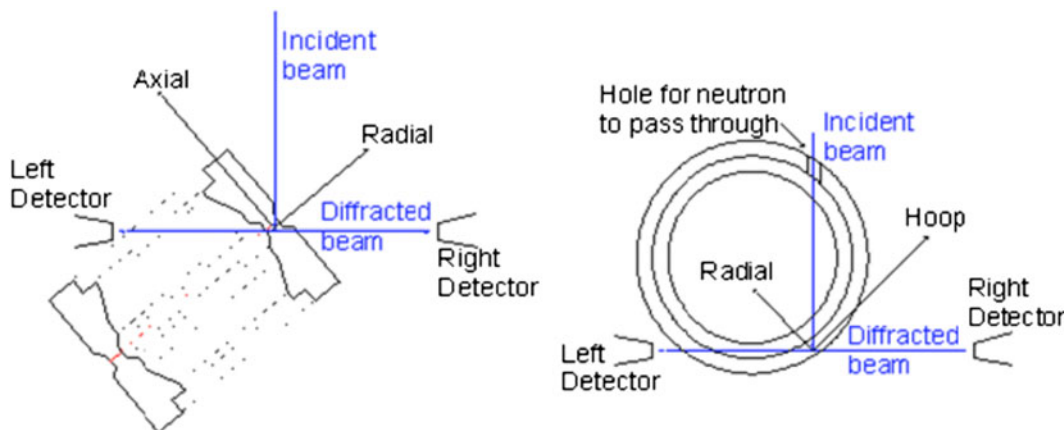


Fig. 3—Schematic describing the setup for measuring strains in the (a) axial, radial and (b) hoop direction. Note that only ENGIN-X has two detectors at a fixed angle of 90 deg, while SALSA and STRESS-SPEC have a single detector but not at a fixed angle.

important to note that previous residual stress characterization of a nickel IFW demonstrated excellent agreement between single peak analysis, carried out at monochromatic beam lines such as SALSA, and multiplex Rietveld analysis carried out at the time-of-flight beam line ENGIN-X.^[19] In the case of reactor sources, a monochromatic neutron beam with a wavelength of about $\lambda = 1.5\text{\AA}$ was used to record the (311) diffraction peak. The diffracting gage volume was defined using slits and collimators. The horizontal gage dimensions were $1.5\text{ mm} \times 1.5\text{ mm}$ at SALSA and $2\text{ mm} \times 2\text{ mm}$ at STRESS SPEC and ENGIN-X. In the case of the radial and hoop directions, it was possible to use a relatively large vertical slit size (10 mm), reducing the necessary counting time to 10 to 15 minutes per point. In order to minimize the path length and facilitate the hoop strain measurements, a small window of $12 \times 12\text{ mm}$ was electrodischarge machined from the weld region of each specimen, at a position distant from the neutron measurement location. The cutting plane was perpendicular to the hoop direction. In the case of the hoop strain measurement, a 2-mm vertical slit size was used in order to have a sufficiently high axial spatial resolution. This resulted in counting times of 50 to 80 minutes for each hoop measurement point depending on the beam line.

The measurement procedure aimed at measuring the strain values across the weld line and at three different sample wall thickness positions. In addition to the stress characterization, some detailed microstructure analysis was carried out across the weld line using scanning electron microscopy (SEM). Electron backscatter diffraction (EBSD) provided band contrast maps to observe the γ grain size variation across the weld line. For all microstructural analyses, small crossweld samples, extracted from the joint, were carefully ground and polished to mirror finish using standard metallographic techniques. The maps were recorded using a FEI XL30 field emission gun SEM operating at 20 kV with a sample working distance of 20 mm and the HKL EBSD system.

III. RESULTS AND DISCUSSION

A. Weld Microstructure

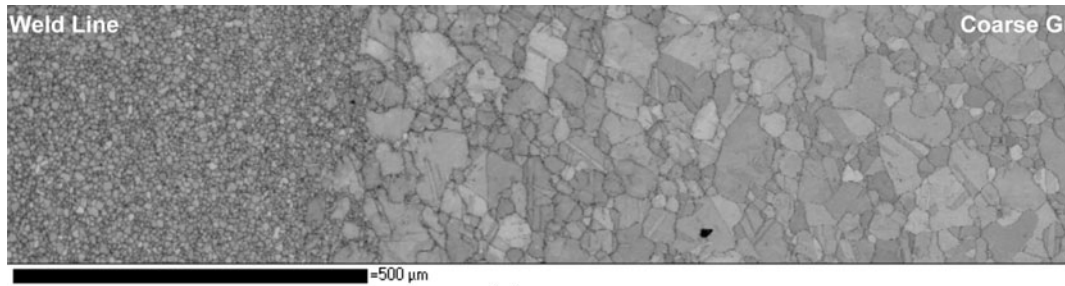
Figures 4(a) and (b) show band contrast maps recorded by EBSD ranging from the weld line toward the parent material of CG and FG RR1000, respectively. Additional grain size analysis further away from the weld line confirmed that no grain size variation was seen beyond the microstructure displayed at the right-hand side of the band contrast images, and a more quantitative analysis of the grain size variation is displayed in Figure 4(c). The mean grain size of parent CG RR1000 is about $30 \pm 5\ \mu\text{m}$, while that of the FG RR1000 parent material is about $7 \pm 2\ \mu\text{m}$. In the case of CG RR1000 IFW, a dramatically reduced grain size is observed within $400\ \mu\text{m}$ from the weld line (Figures 4(a) and (c)). In this region, the material appears to have dynamically recrystallized, resulting in an average grain size of about $6\ \mu\text{m}$. The same grain size

was also found in the weld region of the FG RR1000 weld, which extended to about $400\ \mu\text{m}$ from the weld line (Figure 4(b) shows that the difference between the weld and parent microstructure is hardly noticeable due to the FG size of the parent material). An analysis of the EBSD data in terms of texture development showed no preferred grain orientation in the weld region. Analysis of the γ' distribution within the HAZ of the IFWs also revealed no noticeable differences between CG and FG inertia welded RR1000. In both cases, only reprecipitated γ' (in the range of 10 to 20 nm) was found at the weld line, indicating that the γ' solvus was exceeded during IFW. This demonstrates that even though the parent microstructures of FG and CG RR1000 are quite different, the weld microstructures are very similar in terms of grain size and γ' distribution.

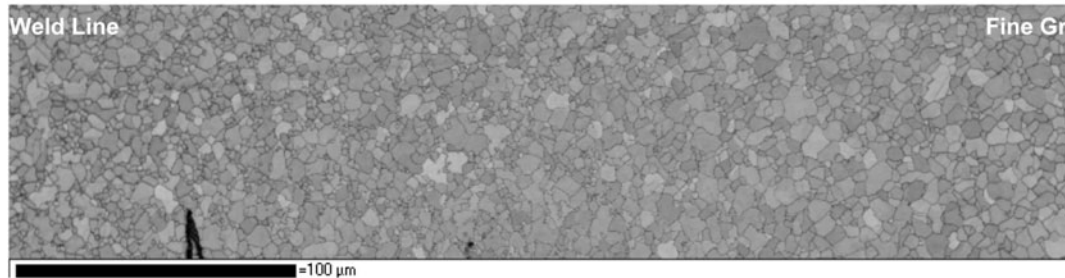
B. Residual Stress Characterization

Figure 5 shows the hoop, radial, and axial stress distribution across the weld line, in sample S1 (CG-AW) at three different sample thickness positions, *i.e.*, 1 mm below the inner surface (ID), at the center of the sample thickness (C), and at 1 mm below the outer surface (OD). As described in the previous paragraph, the axial stresses are balanced for each axial (Z) position. The accuracy of the peak fit can provide an indication of the possible error of the strain and stress analysis. In the present case, radial and axial stress data were estimated to have an accuracy of $\pm 50\text{ MPa}$ and hoop stresses and accuracy of $\pm 100\text{ MPa}$. The maximum tensile stress is found in the hoop direction for the ID and C-line scan and ranges close to 1600 MPa. The stress gradient in the hoop direction is relatively steep, suggesting that zero hoop stresses are reached at about 10 mm from the weld line. There exists a clear stress gradient at the weld line between the positions close to the inner and the outer diameters of the sample, which is related to the bending moment found for the axial stresses.^[5] The axial stresses are very significant for the ID and OD measurements reaching values of +600 MPa for the ID and -600 MPa for the OD line scan. As expected, the radial stresses generally show the least stress values, although some radial stresses in the center of the wall indicate the tendency for a hydrostatic stress field. In Figure 6, the residual stress distribution is plotted for sample S2 (the same type of weld as S1 but after PWHT). After PWHT, the stress magnitudes are reduced most significantly for the hoop direction to a maximum value of about 1000 MPa. The radial stresses are reduced essentially to zero, while the bending moment of the axial stresses is reduced giving maximum axial stresses of $\pm 400\text{ MPa}$.

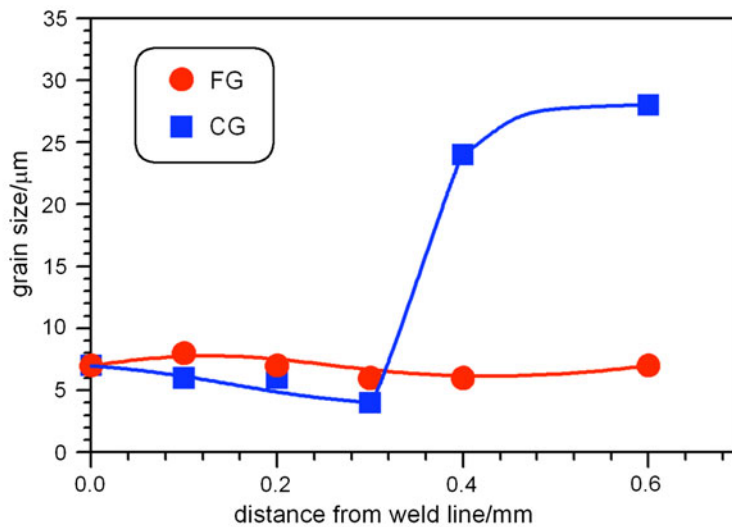
Figures 7 and 8 provide a similar comparison between an as-welded (S3) and postweld heat-treated (S4) FG material. In general, the trends are comparable to CG RR1000. Even though the temperature capability of CG RR1000 is about 303 K (30 °C) higher than that for FG-RR1000,^[11] the hoop stress profiles are broadly comparable. There is certainly no indication that inertia friction welded CG RR1000 displays significantly higher stresses in the HAZ compared to inertia friction welded FG RR1000. The bending moment observed for the



(a)



(b)



(c)

Fig. 4—Band contrast image, recorded by EBSD, displays the γ microstructure variation from the weld line (left edge of the image) toward the base material for (a) CG RR1000 IFW and (b) FG RR1000 IFW.

axial stresses seems to be slightly higher in S3 (FG) compared to S1 (CG). However, it should be kept in mind that these welds were carried out on a development inertia friction welder with unoptimized tooling design. Previous work^[5,6] showed that tool design has a significant effect, particularly on the axial stresses leading to potential scatter between individual weld samples. Since in the present case the gripping of the

weld samples was adjusted manually without any control of the gripping strength, some noticeable variations of axial stresses between weld samples are not surprising.

In order to compare the high residual stresses determined at the weld line to the elastic limit of the material, the equivalent stress was calculated using the following equation:^[20]

$$\sigma_{eq} = \sqrt{0.5 \cdot \left((\sigma_{radial} - \sigma_{axial})^2 + (\sigma_{axial} - \sigma_{hoop})^2 + (\sigma_{hoop} - \sigma_{radial})^2 \right)} \quad [3]$$

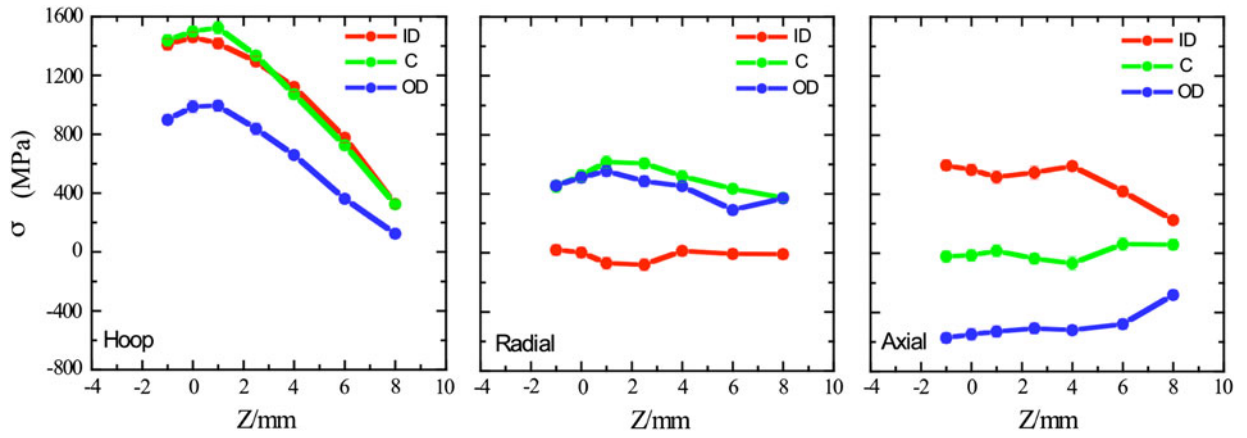


Fig. 5—Hoop, radial, and axial residual stress distribution across the weld line of CG RR1000 IFW in the as-welded condition (sample S1). Z (in mm) is the distance away from the weld line.

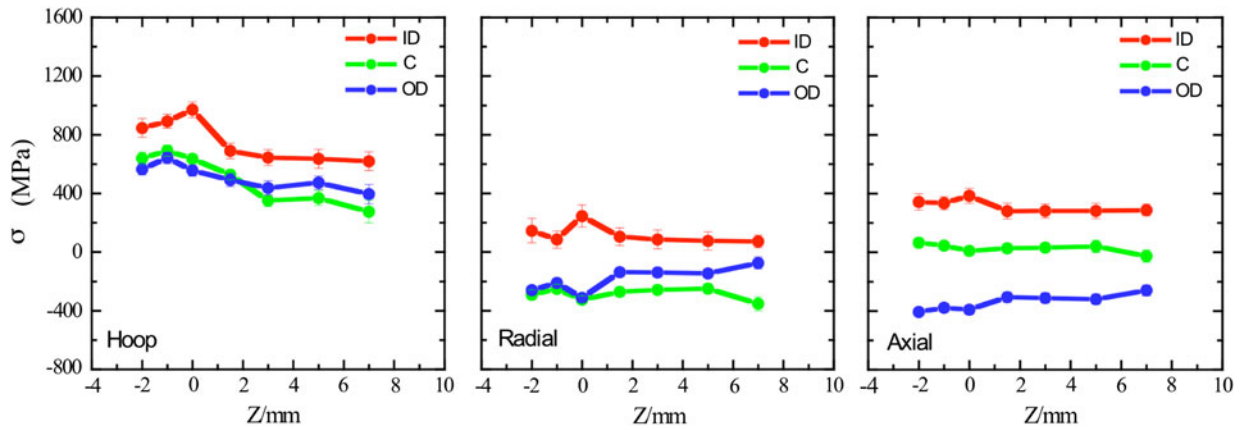


Fig. 6—Hoop, radial, and axial residual stress distribution across the weld line of CG RR1000IFW in the postweld heat-treated condition (sample S2). Z (in mm) is the distance away from the weld line.

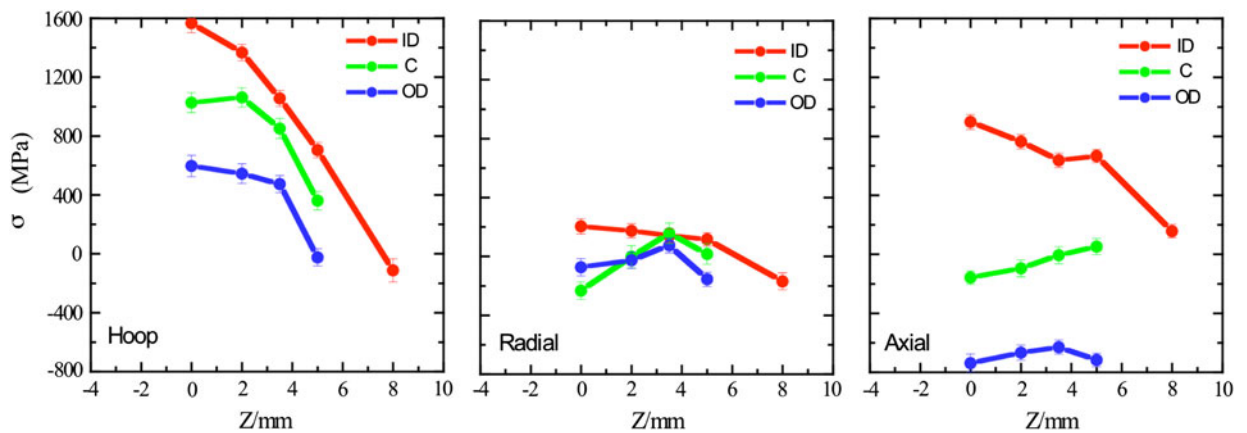


Fig. 7—Hoop, radial, and axial residual stress distribution across the weld line of FG RR1000 IFW in the as-welded condition (sample S3). Z (in mm) is the distance away from the weld line.

The maximum equivalent stresses were calculated at the weld line for the ID measurement point in the range of 1100 to 1200 MPa. This range compares to a 0.2 pct proof stress of about 1100 MPa for RR1000 at room temperature.^[21] This suggests that the residual stresses

generated at the weld line are limited by the yield strength of the material. Previous work demonstrated that the proof stress in RR1000 increases by about 10 to 15 pct in the weld region,^[10] which explains equivalent stresses exceeding 1100 MPa in the weld region here.

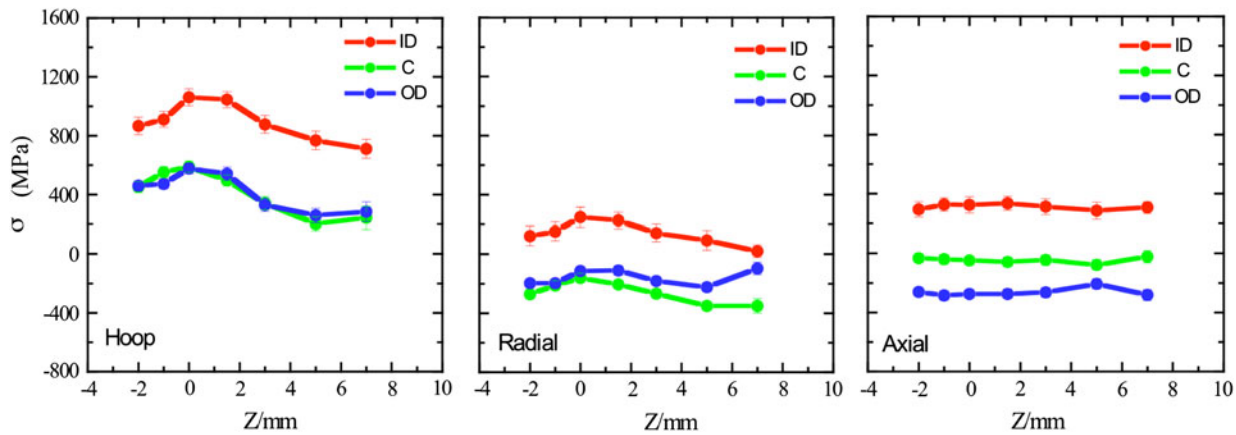


Fig. 8—Hoop, radial, and axial residual stress distribution across the weld line of FG RR1000IFW in the postweld heat-treated condition (sample S4).

Since the weld microstructure of AW S1 (CG) and S3 (FG) are very similar, it is not surprising that the residual stresses are not significantly different. Indeed, Vickers hardnesses at the weld line in S1 and S3 revealed very similar values (500 HV1 in S1 and 470 HV1 in S3). When comparing the effect of the PWHT on CG RR1000 IFW (S2) and FG RR1000 IFW (S4), it seems that no effect of the different parent material conditions on stress mitigation can be identified even though CG RR1000 was reported to have superior creep resistance than FG RR1000.^[11] This suggests that it is the highly stressed weld region that affects stress relief during PWHT in which the microstructure does not significantly differ when comparing the two welds. Since the microstructure was altered dramatically during IFW, the creep properties of the weld microstructure might differ from the parent material. For instance, in the present case, one might expect that in comparison to CG RR1000, the refined grain size at the weld line can help to reduce residual stresses more quickly, while the exceptionally fine γ' distribution in this region is likely to strengthen the material over a wide temperature range and, hence, make stress mitigation more difficult.

IV. CONCLUSIONS

We studied the residual stress distribution across the weld line of inertia friction welded RR1000 samples made from fine- and coarse-grained parent material by using neutron scattering. The results suggest that the weld residual stresses are independent of the starting microstructure of the parent material. The highest stresses of about 1600 MPa were observed in the hoop direction at the weld line near the inner diameter of the wall. By calculating the equivalent stresses in this location, it seems to be clear that these high tensile stresses are constrained by the yield stress of the material. Since the weld microstructures of CG and FG RR1000 IFWs are very similar, the increased temperature capability of CG RR1000 compared to FG RR1000 does not seem to affect the stress profiles generated during welding. The PWHT, applied in the present case, reduced

the residual stresses by about 35 pct on average. Again, no differences were detected between CG and FG RR1000 IFWs in terms of stress relaxation even though CG RR1000 has a higher temperature capability than FG RR1000 and, consequently, might be expected to retain higher residual stresses after PWHT. This demonstrates that most of the stress relaxation comes from the highly stressed weld region where the microstructures of the two welds are very similar.

ACKNOWLEDGMENTS

Part of this research was undertaken in the PANACEA (Processing of an Advanced Nickel Alloy for Critical Engine Applications) Project (TP/4/MHT/1/22012), which forms part of the UK Government Technology Strategy Board Programme. Rolls-Royce plc and Manchester University acknowledge the financial support provided by the Technology Strategy Board. The authors also thank Colin Small, Rolls-Royce plc, for coordination of the PANACEA Project and Rolls-Royce plc for permission to publish this work. The authors also acknowledge the Institute Laue Langevin (Grenoble, France), ISIS (Chilton, United Kingdom), and the FRM II (Munich, Germany) for the provision of the neutron scattering facilities.

REFERENCES

1. C.T. Sims and W.C. Hagel: *The Superalloys*, Wiley, New York, NY, 1972.
2. R.F. Decker: *Climax Symp.*, May 1969, Am. Mit. Climax Inc.
3. M. Preuss, J.W.L. Pang, P.J. Withers, and G.J. Baxter: *Metall. Mater. Trans. A*, 2002, vol. 33A, pp. 3215–25.
4. M.C. Hardy, B. Zirbel, G. Shen, and R. Shankar: *Superalloy 2004*, K.A. Green, T.M. Pollock, H. Harada, J.J. Schirra, and S. Walston, eds., TMS, Warrendale, pp. 83–90.
5. B. Grant, M. Preuss, P.J. Withers, G. Baxter, and M. Rowson: *Mater. Sci. Eng. A*, 2009, vols. 513–514, pp. 366–75.
6. J.W.L. Pang, M. Preuss, P.J. Withers, G.J. Baxter, and C. Small: *Mater. Sci. Eng. A*, 2003, vol. 356 (1–2), pp. 405–13.
7. M. Preuss, J.W.L. Pang, P.J. Withers, and G.J. Baxter: *Metall. Mater. Trans. A*, 2002, vol. 33A, pp. 3227–34.

8. P.J. Withers and M. Preuss: *ASM Handbook*, vol. 22B, *Modeling and Simulation: Processing of Metallic Materials*, D.U. Furrer and S.L. Semiatin, eds., ASM INTERNATIONAL, Materials Park, OH, 2010.
9. B. Grant, M. Preuss, P.J. Withers, G. Baxter, and M. Rowson: *Mater. Sci. Eng. A*, 2009, vols. 513–514, pp. 366–75.
10. M. Preuss, P.J. Withers, and G. Baxter: *Mater. Sci. Eng. A*, 2006, vol. 437 (1), pp. 38–45.
11. R.J. Mitchell, J.A. Lemsky, R. Ramanathan, H.Y. Li, K.M. Perkins, and L.D. Connor: *Superalloy 2008*, R. Reed *et al.*, eds., TMS, Warrendale, pp. 347–56.
12. M.T. Hutchings, P.J. Withers, T.M. Holden, and Torben Lorentzen: *Introduction to Characterization of Residual Stress by Neutron Diffraction*, CRC Press, Boca Raton, FL, 2005.
13. P.J. Withers, M. Preuss, A. Steuwer, and J.W.L. Pang: *J. Appl. Crystallogr.*, 2007, vol. 40 (Part 5), pp. 891–904.
14. M.W. Johnson, L. Edwards, and P.J. Withers: *Physica B*, 1997, vol. 234, pp. 1141–43.
15. I.C. Noyan and J.B. Cohen: *Residual Stress*, Springer Verlag, New York, NY, 1987, p. 111.
16. T. Pirling, G. Bruno, and P.J. Withers: *Mater. Sci. Eng. A*, 2006, vol. 437, pp. 139–44.
17. J.A. Dann, M.R. Daymond, L. Edwards, J.A. James, and J.R. Santisteban: *Physica B*, 2004, vol. 350, pp. 511–14.
18. M. Hofmann, R. Schneider, G.A. Seidl, J. Rebelo-Kornmeier, R.C. Wimpory, U. Garbe, and H.G. Brokmeier: *Physica B*, 2006, vols. 385–386, p. 1035.
19. M. Karadge, B. Grant, G. Bruno, J. Santisteban, P.J. Withers, and M. Preuss: *Mater. Sci. Forum*, 2006, vols. 524–525, pp. 393–98.
20. R. Hill: *The Mathematical Theory of Plasticity*, Oxford Classic Series, Clarendon Press, Oxford, United Kingdom, 1998, p. 26.
21. R.A. Claudio, J.M. Silva, C.M. Branco, and J. Byrne: “Crack Propagation Behaviour of Shot Peened Components at Elevated Temperature,” 10 as Jornadas de Fractura, Univ. do Minho, Portugal, Fevereiro 2006 (available at <http://ltodi.est.ips.pt/rclaudio/>).